Available online at www.sciencedirect.com
SCIENCE DIRECT®

Journal of the European Ceramic Society 24 (2004) 1521–1524

www.elsevier.com/locate/jeurceramsoc

Compositional evolution of structural phase transitions in sodium niobates

B. Jiménez*, R. Jiménez, A. Castro, L. Pardo

Instituto de Ciencia de Materiales de Madrid, CSIC, 28049 Cantoblanco, Madrid, Spain

Abstract

$Li_xNa_{1-x}NbO_3$ ceramics with $5 \leqslant x \leqslant 12\%$ have been studied in the temperature range RT–773 K through elastic, thermal expansion and dielectric measurements as a function of the temperature. Thermal expansion behaviour shows single, (for $x \leqslant 8\%$) or double, (for $x \geqslant 10\%$), reversible anomalies in the complete thermal cycle. The elastic behaviour shows single, for $x = 5\%$, or double and reversible anomalies, for $x \geqslant 8\%$. In both cases the thermal behaviours scarcely depend on the thermal rate. The dielectric permitivity shows reversible single anomalies in the phase transition temperature for $x \leqslant 8\%$ and double non-reversible anomalies for $x \geqslant 8\%$ that are very dependent on the thermal rate and thermal history of the sample. The crossover composition for the appearance of a double anomaly can be established close to $x = 8\%$. The main (FE–PE) phase transitions and their temperatures have been established using three measuring techniques.

Keywords: Ceramics; Ferroelectrics; Phase transitions

1. Introduction

Solid solutions of $Li_xNa_{1-x}NbO_3$, have become very interesting materials for microwave, pyroelectric and nowadays for piezoelectric applications to substitute lead containing piezoelectrics, like PZT, for many technological applications.

These compounds have a perovskite type structure and present several structural phase transitions.[1,2] At room temperature the compositions with $x \leqslant 2\%$ are antiferroelectric and those with $x \geqslant 2\%$ are ferroelectric.

The large thermal hysteresis appearing in the phase transitions of the RT–773 K temperature range have been attributed to the coexistence of antiferroelectric (AFE) and ferroelectric (FE) phases: AFE–FE[1] ($x \leqslant 2\%$) and FE–FE[3,4] ($x \geqslant 12\%$). The very recently found[5] low temperature phase transition for $x = 0$ is considered as AFE–AFE phase transition.

It has been suggested,[6] after diffraction studies, that only the composition ranges

(1) $0 \leqslant x \leqslant 5\%$, (2) $12\% \leqslant x \leqslant 23\%$, (3) $23\% \leqslant x \leqslant 100\%$

present clear solid solutions, but other studies[2] do not agree with such a considerations.

Studies on single crystals of the $x = 9\%$ composition[7] in the RT–773 K temperature range present a unique peak in dielectric constant at the phase transition temperature (658 K). In compositions with $x = 12\%$ and $x = 15\%$ several peaks in the dielectric constant were found in the heating measuring run, but a unique wide peak in the cooling one.[3,4]

The aim of this work is to provide information on the possible structural phase transitions of the $5 \leqslant x \leqslant 12\%$ compositions in the RT–773 K temperature range where some discrepancy seems to exist[2,6] by studying their elastic, thermal expansion and dielectric properties.

2. Experimental procedure

Ceramics of sodium-lithium niobates have been prepared by sintering of the precursors obtained by solid state chemical reaction of stoichiometric mixtures of the component oxides and carbonates of nominal composition $Li_xNa_{(1-x)}Nb\ O_3$, here after LNN(x), with $x = 5$–8–10 and 12%.

The precursors were characterized by X-ray powder diffraction technique. XRD recordings were performed

* Corresponding author. Tel.: +34-91-334-9000; fax: +34-91-372-0623.
E-mail address: basilio.jimenez@icmm.csic.es (B. Jiménez).

0955-2219/$ - see front matter © 2003 Published by Elsevier Ltd.
doi:10.1016/S0955-2219(03)00532-6

at room temperature with scan rate of 1° (2θ) per minute (Siemens D500) using Cu K_α radiation ($\lambda = 1.5418$ Å).

Ceramics with 90–93% densification were obtained by sintering pellets in air at 1225 °C during 3 h.

Dielectric measurements as a function of the temperature were performed with a HP4194A Impedance Analyser at 2 °C/min temperature rate. Sputtered platinum or platinum paste were used to electrode the samples.

Mechano elastic measurements were achieved by the Three Point Bending technique as it is described elsewhere[8] on samples of 12.00×2.00×0.35 mm. The temperature of the sample was varied at a rate of 2 °C/min in a continuous way. The same samples and temperature rates as for TPB were used for thermal expansion measurements.

3. Experimental results

Elastic, thermal expansion and dielectric constant measurements as a function of the temperature were performed in the prepared compositions in the RT–773 K temperature range. XRD patterns at room temperature were also obtained.

3.1. X-ray

The X-ray diffraction patterns clearly indicate that the corresponding solid solutions are formed in all compositions. These are isostructural with $NaNbO_3$ (JCPDS 33-1270), unit-cell parameters close to $a = 5.568\%$, $b = 15.52\%$ and $c = 5.504\%$, belonging to the Pbma (No 57) space group. In Fig. 1 the X-ray patterns for different compositions, included for $x = 0$, are shown. The diffractograms are very similar and single phases seem to be present in all the cases.

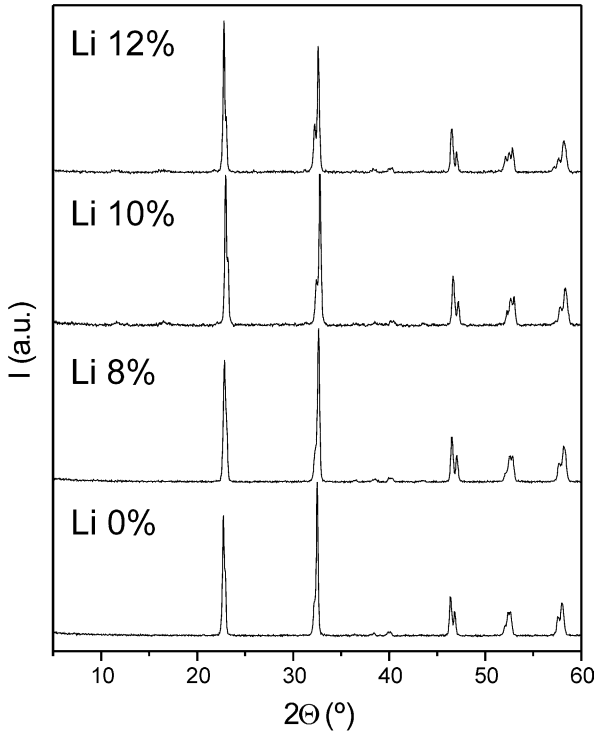

Fig. 1. Powder XRD for LNN(5,8,10,12) compositions.

3.2. Piezoelectric

Piezoelectric coefficient d_{33} measured at room temperature in poled samples with the d_{33}-Berlincourt Meter provide values in the range 30pC/N–45pC/N, variations mainly depending on the samples densification rather than on their composition.

3.3. Elastic

In Figs. 2 and 3 we plot the relative, $Y/Y_{673\ K}$, Young's modulus and mechanical loss tangent, $\tan\delta_m \times 10^{-2}$, as a function of the temperature for compositions LNN(5), LNN(8), LNN(10) and LNN(12). The anomalies are marked in the plots with their respective temperatures.

In all cases besides the main narrow peak in $\tan\delta_m$ and narrow minimum in the Young's modulus, wide maxima/minima, respectively, are found at lower temperatures. In the $x \geqslant 10\%$ compositions the minimum at lower temperature than that of the main one is very well defined.

In Table 1 the temperatures of the minimum of the Young's modulus and those of $\tan\delta_m$ narrow peaks for all the studied compositions are shown. Since a thermal hysteresis was found, the values for the heating (H) and cooling (C) runs are indicated.

3.4. Thermal expansion

In Fig. 4 we plot the complete thermal cycle (heating–cooling) of thermal expansion for LNN(5,8,10,12) compositions. To strengthen the anomalies we have subtracted from the experimental data the linear parts

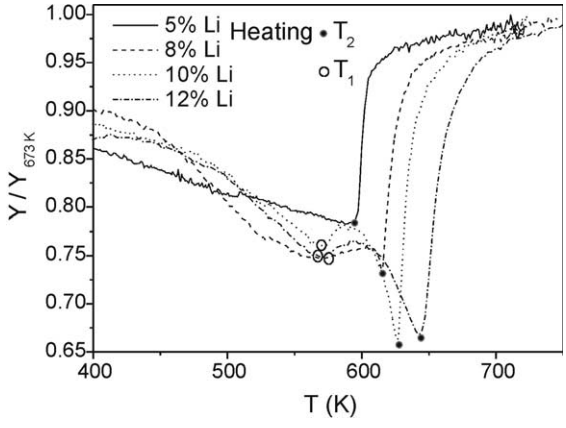

Fig. 2. Relative Y/Y_{673K} as a function of the temperature on heating for LNN(5,8,10,12) compositions. Black points mark the temperature T_2, small circles mark the temperature T_1.

of L(T) below the anomalies. The results show that the anomalies occur at temperatures in the interval 513–573 K.

The samples with $x \geqslant 10\%$ present two clear reversible anomalies, but those with $x < 10\%$ present only one reversible anomaly.

In Table 2 the temperatures of the anomalies in the heating (H) and cooling (C) runs for the studied compositions are given.

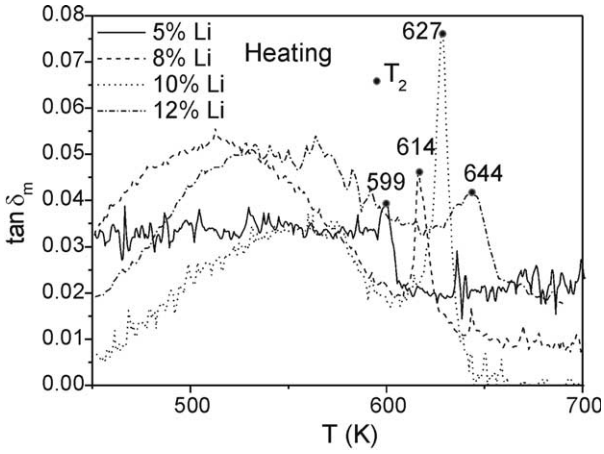

Fig. 3. Mechanical loss tangent, $\tan\delta_m$, as a function of the temperature on heating for LNN(5,8,10,12) compositions. Black points mark the temperature T_2.

Table 1
Temperatures (K) of mechano-elastic anomalies

x(%)	T_1(H)	T_1(C)	T_2(H)	T_2(C)
5			599	570
8	572	573	616	606
10	572	563	627	617
12	573	558	644	619

H = Heating. C = Cooling. T_1 = Lower temperature anomaly. T_2 = Higher temperature anomaly.

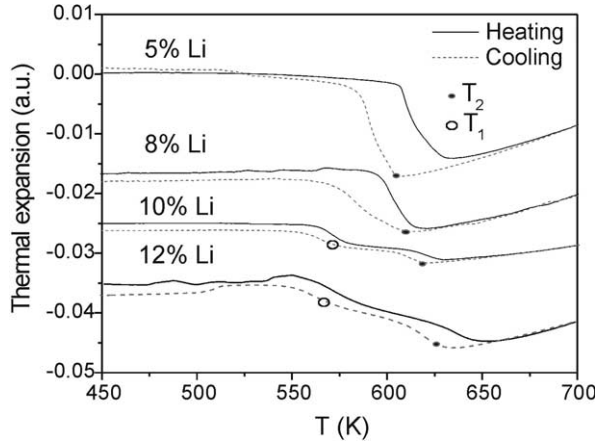

Fig. 4. Thermal expansion in arbitrary units as a function of the temperature on heating–cooling for LNN(5,8,10,12) compositions. The curves have been corrected to stand out the anomalies. Black points mark the temperature T_2, small circles mark the temperature T_1.

3.5. Dielectric

The results obtained for LNN(5,8,10,12) compositions for heating and cooling run are shown in the Figs. 5 and 6, respectively. We observe a main peak for all the compositions and some other anomalies for samples LNN(10,12). In all the cases there is an important thermal hysteresis.

Table 2
Temperatures (K) of thermal expansion anomalies

x(%)	T_1 (H)	T_1 (C)	T_2(H)	T_2 (C)
5			624	605
8			618	610
10	585	571	628	618
12	588	567	642	625

H = Heating. C = Cooling. T_1 = Lower temperature anomaly. T_2 = Higher temperature anomaly.

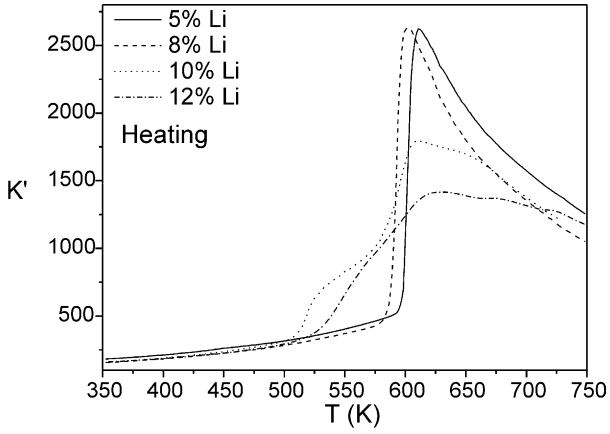

Fig. 5. Dielectric constant as a function of the temperature on heating for LNN(5,8,10,12) compositions.

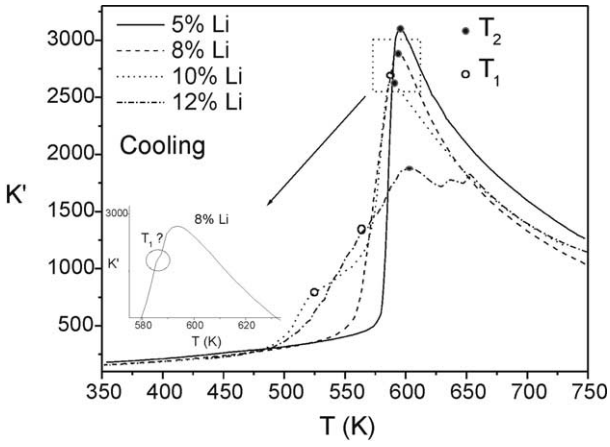

Fig. 6. Dielectric constant as a function of the temperature on cooling for LNN(5,8,10,12) compositions. Black points mark the temperature T_2, small circles mark the temperature T_1.

Table 3
Temperatures of dielectric anomalies

x(%)	T_1 (H)	T_1 (C)	T_2(H)	T_2 (C)
5			613	595
8	587?		601	593
10	525	520	603	589
12	565	560	625	602

H = Heating. C = Cooling. T_1 = Lower temperature anomaly. T_2 = Higher temperature anomaly.

The temperatures of the more significant dielectric anomalies are presented in Table 3.

4. Discussion

On the basis of elastic and thermal expansion results two main anomalies can be defined in the temperature interval RT–773 K, at the temperatures T_1 and T_2 ($T_1 < T_2$) for samples LNN(10) and LNN(12) and only one at T_2 for LNN(5) and LNN(8). At T_2 the main mechano elastic anomalies take place in all the compositions. Dielectric constant results show the main peaks at T_2 for all the compositions, but samples LNN(10) and LNN(12) present additional not quite reversible elbows or peaks below and above T_2. The temperature T_1 can be defined in both samples if we take into account elastic and thermal expansion results and the elbows of ε'(T) curves below T_2. In the LNN(8) composition we can observe different slopes in the heating than in the cooling run curves as compared with those of LNN(5) sample. An incipient anomaly is observed at a temperature (let us say T_1) below that of the main peak at T_2 in the cooling run curve (inset of Fig. 6).

The temperatures of dielectric anomalies are, in general, lower than those in the other two used experimental techniques and depend on the temperature measuring rates.

These facts lead us to consider that the anomalies at T_2 should correspond to FE–PE phase transitions in all the studied compositions because these phase transitions enclose important dimensional changes, revealed by thermal expansion measurements and strain-order parameter coupling,[9,10] revealed by elastic measurements. For $x \geqslant 10\%$, the anomaly at T_1 suggests a FE–FE phase transition with dimensional and ferroelectric polarization changes.

The composition $x = 8\%$ with its emerging second anomaly at a temperature lower than that of the main peak (T_2) in the dielectric constant and mechano elastic curves should be chosen as the crossover composition to separate single from double stable anomaly compositions.

5. Conclusions

X-ray diffraction patterns of Li–Na niobates with Li in the $5 \leqslant x \leqslant 12\%$ range show that these compositions form solid solutions, no mixture of phases was observed by XRD.

The LNN(5) composition shows a unique structural FE–PE phase transition, in the 500–750 K temperature interval at the temperature T_2. For LNN(8) composition mechano elastic and dielectric results reveal an small anomaly that could indicate an incipient FE–FE phase transition (T_1) besides the main FE–PE at T_2. This composition can be considered as the crossover one for compositions with one or two phase transition in the studied temperature interval. Compositions with $x \geqslant 10\%$ show two phase transitions temperatures T_1(FE–FE) and T_2,(FE–PE) below 773 K.

The use of the three techniques provides an effective tool to ascribe some anomalies in the corresponding properties of the studied compounds to structural FE–FE or FE–PE phase transitions.

Acknowledgements

The authors thank Ms. M. Antón for sample preparation. This work has been performed through the Project LEAF G5RD-CT-2001-00431 financed by EU.

References

1. Sadel, A., Von der Mühll, R. and Ravez, J., *Mat. Res. Bull.*, 1983, **18**, 45.
2. Von der Mühll, R., Sadel, A., Ravez, J. and Hagenmüller, P., *Solid State Comm.*, 1979, **31**, 151.
3. Nobre, M. A. L. and Lanfredi, S., *J. Phys. Chem. Solids*, 2001, **62**, 1999.
4. Nobre, M. A. L. and Lanfredi, S. J., *Phys.: Conden. Matter.*, 2000, **12**, 7833.
5. Lanfredi, S., Lente, M. H. and Eiras, J. A., *Appl. Phys. Letters*, 2002, **80**, 2731.
6. Lacomte, J. and Quemeneur, E., *Bull. Soc. Chem. France*, 1974, **12**, 2779.
7. Song, Y., Chen, H., Chen, F., Sun, D., Zhang, P. and Zhong, W. J., *Synthetic Crystals*, 1989, **18**(2), 117.
8. Jiménez, B. and Vicente, J. M., *J. Phys. D: Appl. Phys.*, 1998, **31**, 446.
9. Kityk, A. V., Schranz, W., Sondergeld, P., Havlik, D., Saljeand, E. K. H. and Scott, J. F., *Phys. Rev. B*, 2000, **61**, 946.
10. Jiménez, B. and Jiménez, R., *Phys. Rev. B*, 2002, **66**.